Chapter 2
Surface Science Studies of Metal Oxide Gas Sensing Materials

Junguang Tao and Matthias Batzill

Abstract In this chapter we present recent advances in the study of metal oxide surfaces and put them in relation to gas sensing properties. A reoccurring scheme is the dependence of chemical surface properties on the crystallographic orientation of the surface. This dependence will become more important in gas sensing applications as nanomaterials with controlled crystal shapes are being designed. In particular we focus on differences of the surface properties of the two polar surfaces of ZnO and the two most abundant bulk terminations of rutile TiO_2, i.e. the (110) and (011) crystallographic orientations. On the example of these metal oxides, we describe the use of vacuum based surface science techniques, especially scanning tunneling microscopy and photoemission spectroscopy, to obtain structural, chemical, and electronic information.

2.1 Relation Between Metal Oxide Gas Sensors and Surface Science

Semiconducting metal oxides can exhibit a conductivity change due to the adsorption or reactions of molecules from the gas phase with the surface. Monitoring this conductivity change enables the use of this information as a gas response signal. The change in conductivity is brought about by an upward or downward shift of the Fermi-level within the band-gap of these predominantly n-type materials. The Fermi-level shift may be induced by charge transfer from the gas sensing material to an adsorbate. For macroscopic materials this induces a

J. Tao · M. Batzill (✉)
Department of Physics, University of South Florida, Tampa 33620, USA
e-mail: mbatzill@usf.edu

M. A. Carpenter et al. (eds.), *Metal Oxide Nanomaterials for Chemical Sensors*, Integrated Analytical Systems, DOI: 10.1007/978-1-4614-5395-6_2,

band bending at the surface while for microscopic particles (smaller than the Debye screening length) the Fermi-level within the entire particle shifts. Such adsorbate induced shifts of the Fermi-level are dominant for surface sensitive gas sensing materials such as SnO_2 and ZnO. Another mechanism that can result in the shift of the Fermi-level is a variation of the bulk dopant concentration. For example, Ti-interstitials and oxygen vacancies in the bulk of TiO_2 act as intrinsic n-type dopants. The concentration of these dopants depends on the oxidation potential of the surrounding gas phase and the surface of the TiO_2 may act as a source or sink of Ti-interstitials for the bulk.

Clearly, gas sensing with semiconducting metal oxides is initiated by molecular interaction with surfaces and surface science studies therefore have played an important role in the understanding and describing of the fundamental mechanisms [1]. Recent advances in surface science now allow a molecular scale description of metal oxide surfaces and this has provided many new fundamental insights on the properties of these materials. Traditional surface science studies make two important simplifications to the general complex morphology of gas sensing materials; (1) macroscopic single crystalline materials (usually bulk samples but sometimes also high quality epitaxial thin films may be used) are studied, and (2) the surfaces are prepared and investigated under well-controlled ultra high vacuum (UHV) conditions. The consequences of these simplifications are that in surface science experiments on macroscopic single crystal samples, no size effects and no interface effects are observed. Furthermore, because the surfaces are generally prepared in vacuum, they are exposed to a reducing environment. In return for the loss of the 'real' gas sensing environment we gain control over crystallographic orientation and surface composition. Furthermore, we have the full arsenal of surface science techniques at our disposal for a detailed surface analysis. Therefore, surface science studies can address critical fundamental questions like: What role does the surface structure play in the adsorption of certain molecules, i.e. do different crystallographic orientations of the same material exhibit different gas sensitivities? What are the sites for molecule adsorption? and consequently, can these sites be controlled to obtain better sensitivity and selectivity? What is the electronic response of the surface upon molecule adsorption or reaction with the surface? Modern surface science studies can provide rich information on the atomic scale surface properties, which is not easily accessible by other methods.

Detailed reviews on surface science studies of SnO_2 have been recently published by one of the authors of this article [2–4] and interested readers are referred to those texts. Here we focus on recent studies mainly done in the authors' laboratory on the two common metal oxide gas sensing materials ZnO and TiO_2. On ZnO we demonstrate the use of high energy-resolution photoemission studies to obtain information on the fundamental stabilization mechanisms of polar surfaces and in particular investigate the role of hydrogen adsorption on different surface orientations. We also illustrate the power of photoemission spectroscopy to gain information on gas sensing reactions on the example of ZnO reacting with H_2S, a common gas sensing application. In the second part we study two surfaces of rutile TiO_2 and show that the surface structure strongly affects the adsorption of

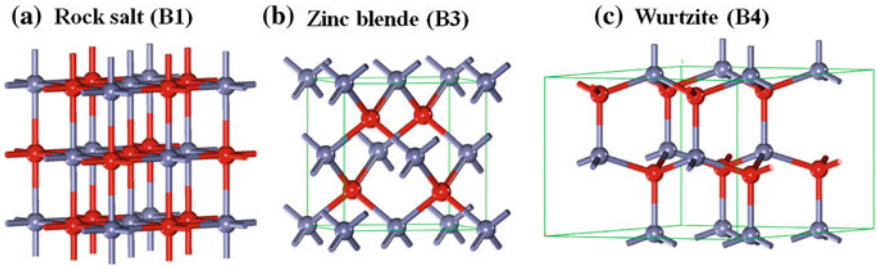

Fig. 2.1 Ball and stick representation of ZnO crystal structures. The *gray balls* are zinc atoms and the *red* ones are oxygen atoms

molecules on the example of acetic acid. In an attempt to modify surface structures and to "engineer" specific surface sites we discuss the use of grazing incidence ion irradiation to create step edges at planar surfaces. Finally, we turn to the oxidation reaction of TiO_2, which demonstrates the mechanism by which the intrinsic bulk dopant concentration is altered.

2.2 ZnO Surfaces

ZnO oxide is one of the prototypical metal oxide gas sensing materials. Its properties have obtained a lot of early attention in the surface science community and have been recently revisited [5]. Its current popularity is also related to the many different nano-structural forms and shapes ZnO self-organizes in under various growth conditions. ZnO crystallizes in three forms: cubic zinc-blende, hexagonal wurtzite and the rarely observed cubic rocksalt structure, which are schematically shown in Fig. 2.1.

Wurtzite is the thermodynamically favored form of ZnO at ambient conditions and zinc blende can be stabilized by growth on cubic substrates, while the rocksalt structure is a high-pressure meta-stable phase. The lattice constants of wurtzite ZnO are $a = 3.25$ Å and $c = 5.2$ Å. This hexagonal lattice consists of two interconnecting hexagonal-close-packed (hcp) sub-lattices of Zn^{2+} and O^{2-}, with each anion surrounded by four cations at the corners of a tetrahedron, and vice versa. The tetrahedral coordination of Zn and O is typical of sp^3 covalent bonding. The ionic character of the material gives rise to a polar repeat-unit along the *c*-axis. As a consequence of this polar symmetry, the (0001) and the (000$\bar{1}$) surfaces of wurtzite ZnO exhibit different bulk terminations, with the first one terminated by Zn-atoms and the latter by O-atoms. This means that if we cleave a crystal along the (0001) plane we obtain two distinctively different surfaces. Importantly, because the repeat unit of the crystal structure perpendicular to these surfaces (along the c-axis) exhibits a dipole moment the Madelung-energy would diverge at these surfaces for an ideal bulk truncation. This is a general property of 'polar

surfaces' and consequently such bulk truncated surfaces cannot be stable. Despite this inherent instability, the polar (0001) and the (0001) surfaces are among the most common crystal orientations of ZnO. This implies that there exist efficient stabilization mechanisms of these surfaces that allow a convergence of the Madelung energy (electrostatic potential). These stabilization mechanisms may also influence the gas sensing properties of ZnO and this is discussed in detail below. Other non-polar surface orientations of wurtzite are the (1120) (*a*-axis) and (1010) faces. The (1010) and (1120) surfaces are the prism faces and the (1121) surface is the pyramid face of the crystal. The non-polar ZnO(1010) surface contain equal number of Zn and O ions and has also been studied extensively by surface science methods because at this surface the coordination of the surface atoms is reduced from fourfold to threefold, thereby creating dangling bonds at the surface which makes it chemically active. Here we focus on the polar surfaces.

2.2.1 The Polar ZnO Surfaces

The two polar surfaces of ZnO are known to have different chemical and physical properties [6]. To stabilize polar surfaces, additional positive or negative charges are required to transfer to the ZnO(000 1)-O or ZnO(0001)-Zn surfaces, respectively. This can be accomplished by removal of lattice ions (surface reconstructions), formation of electronic surface states, or adsorption of impurities such as hydrogen. In the absence of any compositional and structural surface variations a metallization of the surface will occur, i.e. the Fermi-level will be pushed into the valence or conduction band. As shown in Fig. 2.2a, the electrostatic potential introduced by the internal dipole moments causes a shift of the electronic levels relative to the Fermi level in opposite directions at the two polar surfaces, see Fig. 2.2b. Once the conduction band (CB) on one side and the valence band (VB) on the opposite side of the crystal intersect the Fermi level, charges are redistributed from one side to the other. This results in a potential opposing a divergence of the surface potential due to the lattice dipole. In this simplified scheme, the potential due to the internal dipole causes a shift of the energy levels relative to the Fermi level until the VB is depleted on one side and the CB filled on the opposite side. Conceptually, this would result in a charge transfer from one side to the other and thus a potential build up that counteracts the lattice dipoles. However, such a surface metallization is energetically quite expensive and therefore polar surfaces usually stabilize by removing ionic surface charges, i.e. they form surface reconstructions with an altered surface composition compared to the bulk truncation. Such a stabilization mechanism exists for the ZnO(0001)-Zn surface. For the ZnO(000 1)-O surface, on the other hand, it is still debated if a stabilization of this surface by removal of ionic charges exist. This debate may however, mainly be of fundamental scientific interest, since under most realistic environmental conditions it appears that the O-side of the ZnO polar surfaces is terminated by hydrogen and the protons provide the necessary positive charges to converge the

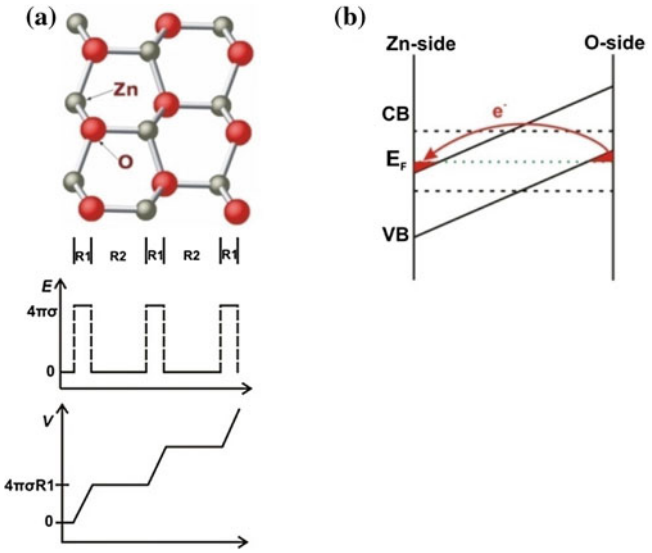

Fig. 2.2 **a** Spatial variation of the Electric Field *E* and of the electrostatic potential *V* in a sample cut along a polar direction where σ is the charge density on the planes. **b** Schematic of surface metallization. Reproduced from Ref. [7]. Copyright 2008, American Physical Society

Madelung energy. The stabilization mechanisms of the polar two surfaces are discussed next.

2.2.1.1 The ZnO(0001)-Zn Polar Surface

The surface structure of the ZnO(0001)-Zn surface prepared in UHV has been thoroughly analyzed by scanning tunneling microscopy and the typical surface morphology is shown in Fig. 2.3a. These measurements resulted in the conclusion that this polar surface is stabilized by removal of $\sim$1/4 ML of Zn atoms from the surface in a *non-periodic* manner [8]. This is achieved by formation of high density of triangular shaped pits and ad-islands that exhibit step edges that are O-terminated as shown in Fig. 2.3b. Thus the Zn-terminated surface under UHV conditions is stabilized by a net removal of positive cations. The formation of sub-stoichiometric polar surfaces is common for the stabilization of many polar materials, however, what makes the ZnO(0001)-Zn surface special, is that it does not involve a periodic surface reconstruction and therefore this stabilization mechanism evaded detection by surface diffraction techniques for a long time. In addition to the direct visualization of the surface structure by STM, high resolution core-level photoemission spectroscopy of ionic surfaces also contains information of the coordination environment in ionic crystals. This is because the core-level binding energy measured in XPS contains a contribution of the Madelung energy at the site of the photoelectron emitting atom [9]. Surface-terrace and step-edge atoms have

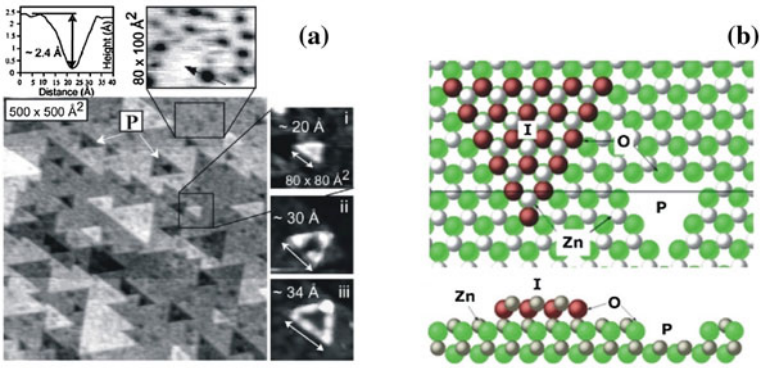

Fig. 2.3 Surface structure of ZnO(0001)-Zn. **a** STM image of surface structure, reprinted with permission from Ref. [8]. Copyright 2003, American Physical Society. **b** Ball model of *top* and cross-sectional view of the ZnO(0001)-Zn surface showing triangular pits (P) and islands (I). The step edges exhibit 3-fold coordinated oxygen atoms compared to the 4-fold coordination on the terraces. Reproduced from Ref. [7]. Copyright 2008, American Physical Society

different Madelung energy than bulk ions, due to their reduced coordination numbers. Therefore photoemitted electrons from different oxygen sites (step-edge, terrace, and bulk) on the ZnO(0001)-Zn surface exhibit slightly different binding energies and this may be used to verify the high density of O-terminated step edges on the vacuum prepared ZnO surface. Using *soft* x-ray photoemission a high surface sensitivity is obtained that enables to observe the binding energy shifts due to the high density of step edges. A de-convolution of the O-1s peak into its different components is shown in Fig. 2.4. A test to demonstrate that the different components are due to the Madelung shift at the surface is to passivate the surface with ZnS (this is discussed in detail below). Such a passivated surface exhibits a narrower O-1s peak because the (shifted) surface contributions are missing. Therefore, the detailed analysis of the O-1s peak shape in soft- x-ray photoemission studies is an elegant confirmation that this surface is stabilized by the formation of a high density of oxygen-terminated step edges in vacuum.

Although formation of high concentration of O-terminated step edges is the stabilization mechanism in vacuum, the stabilization of this polar surface in the presence of different gaseous environments may be achieved by various adsorbates. Different surface terminations have been for example predicted by ab-intio thermodynamics calculations for different hydrogen chemical potentials of the gas phase [8, 10]. Also recent STM studies of ZnO(0001)-Zn surface for exposure to water in vacuum showed that the triangular step edge structure disappears [11], indicating that even at the low water vapor pressure achievable in UHV alternative surface stabilization mechanisms by surface adsorbates become dominant. Furthermore, studies in aqueous solutions have shown that a hydroxide stabilized surface is obtained for pH values between 11 and 4 [12]. Therefore, different environments can strongly affect the surface structure and composition of metal

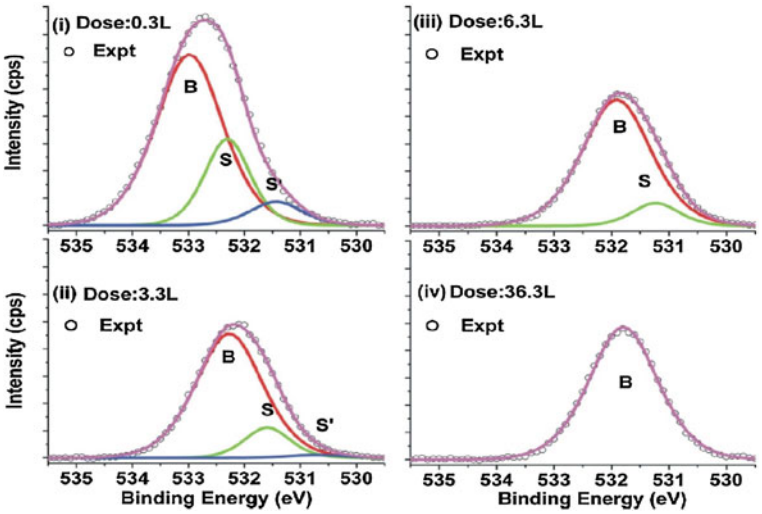

Fig. 2.4 Soft x-ray photoemission spectra of the O-1s peak on ZnO(0001)-Zn surfaces for different amount of surface passivation with ZnS. The O-1s peak can be de-convoluted into three contributions: bulk (*B*), surface terraces (4-fold coordinated) (*S*) and surface step-edge sites (3-fold coordinated oxygen) (*S'*). With increasing surface passivation the surface contribution in the O-1s signal diminishes. Reproduced from Ref. [7]. Copyright 2008, American Physical Society

oxide surfaces. Future surface science studies in other environments than UHV will be needed to advance the understanding of the role of environmental conditions on the surface properties.

2.2.1.2 The ZnO(0001)- O Polar Surface

While the stabilization of the polar ZnO(0001)-Zn surface is quite reasonably explained by removal of ¼ ML of Zn and formation of O-terminated step edges, the stabilization of the ZnO(000 1)-O polar surface is not fully understood yet. Kunat et al. observed a 1 × 3 surface reconstruction for a clean surface, which they interpreted as an ordered array of O-vacancies with 1/3 oxygen atoms missing [13]. This structure, however, does not entirely satisfy the electrostatic stabilization criteria (which requires ¼ ML of missing oxygen) and density functional theory (DFT) calculations have shown that it is not a stable surface structure [14]. Soft x-ray photoemission studies of the O-1s core level [7], shown in Fig. 2.5 have revealed the presence of OH on this surface below ∼300 °C. The hydrogen could only be removed by annealing and holding the sample at temperatures above 300 °C. At this higher temperature, in the absence of hydroxyl groups, an upward band bending was observed, i.e. the Fermi-level was pushed into the band gap towards the valence band. This is reminiscent of the shift in the Fermi-level expected for an unreconstructed, adsorbate free surface as discussed in Fig. 2.2b.

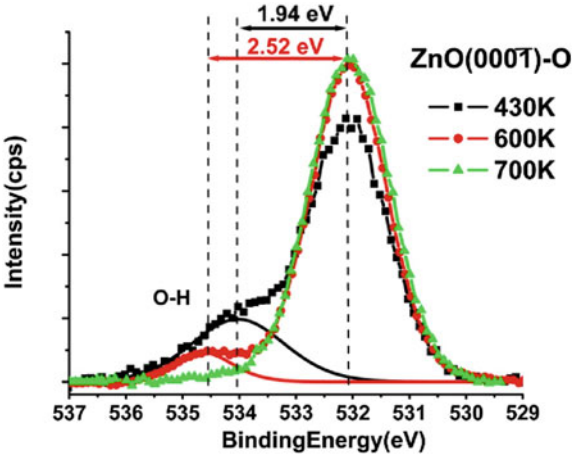

Fig. 2.5 O-1s core level photoemission spectra of the ZnO(000-1)-O surface at different sample temperatures. Only at 700 K a contribution due to surface hydroxyls has completely vanished. At lower temperatures OH groups were always detected. The binding energy of the OH group appears to shift with increasing hydrogen coverage. Reproduced from Ref. [7]. Copyright 2008, American Physical Society

However, the down-ward shift of the Fermi-level was not sufficient to actually remove electrons from the valence band. Nevertheless, especially at elevated temperatures (thermally excited) charge carriers (electrons) are depleted from the surface region by moving the Fermi-level and this can contribute to the electrostatic stabilization of the O-terminated surface. Therefore these soft x-ray photoemission studies demonstrated two important facts. Firstly, at room temperature, even under UHV conditions, the polar surface is likely (partially) hydrogen terminated and secondly, if the surface is hydrogen free (at elevated temperature) this surface is not (completely) stabilized by removal of O-ions and consequently causing a shift in the Fermi-level.

As the photoemission studies showed, hydrogen adsorption on this surface plays an important role. This obviously will affect the adsorption of molecules and thus the gas sensitivity. It is also interesting to point out that recent angle-resolved ultra violet photoemission (ARUPS) studies demonstrated the metallization of this surface due to the presence of hydrogen. ARUPS measurements of the hydrogen induced dispersed surface state at low temperatures are shown in Fig. 2.6. This metallization is due to occupation of ZnO-states in the conduction band from electrons donated from the adsorbed hydrogen [15], i.e. pushing the Fermi-level into the conduction band of ZnO and thus demonstrating a truly metallic electronic surface structure. It is important to point out though that this metallization is different to the purely electrostatic metallization due to the internal dipole moments of ZnO discussed in Fig. 2.2. In case of hydrogen adsorption the metallization is brought about by electron donation from the adsorbed hydrogen and is not in response to the stabilization of the polar surface. Consequently, similar results for surface metallization by hydrogen adsorption can also be obtained for example for the non-polar ZnO(10–10) surface [16].

In terms of gas sensing of ZnO surfaces, surface science studies have shown that the two polar surfaces behave very differently and thus a variation in the gas response is expected for molecular adsorption. Hydrogen may be inadvertently

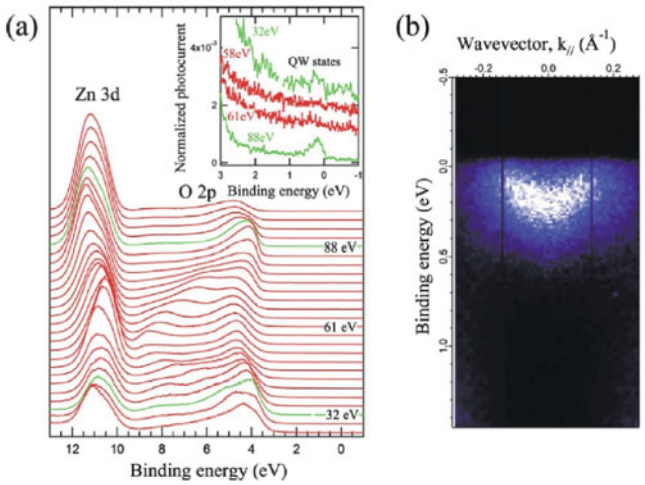

Fig. 2.6 ARUPS studies of ZnO(000-1)-O surface in the presence of hydrogen adsorbates. **a** Normal photoemission studies with the inset showing electronic states at the Fermi-level at 32 and 88 eV photon-energies, which corresponds to the Γ-point in the surface normal direction of the k-vector. **b** ARUPS photocurrent intensity measurement of the near Fermi-level emission for 90 eV photon energy along the direction. Reprinted with permission from Ref. [15]. Copyright 2010, American Physical Society

present on the O-terminated side while the Zn-terminated side is more likely to be hydrogen-free. The easy hydroxylation of the ZnO(000 1)-O causes a metallization of the surface which can affect the conductivity response of such samples. The studies of the surface properties of the polar surfaces indicate that the differences in the chemical properties of the two polar surfaces affects the chemisorption of molecules and this plays an important role in gas sensing of such systems. However, in gas sensing applications where a more drastic surface restructuring occurs, due to *reactions* of the ZnO with gas phase species, the surface orientation plays less of a role in the gas sensitivity. This is for example the case of H_2S sensing with ZnO, which is discussed in the next section.

2.2.2 Surface Reaction of ZnO with H_2S

Detection of hydrogen sulfide (H_2S) is one of the classic applications of metal oxide gas sensors. The gas sensing mechanism can be probed elegantly by surface science studies on single crystal ZnO under UHV conditions. In these studies ZnO is exposed to low background pressures of H_2S (10^{-6} Torr) within the vacuum chamber where the structural, compositional and electronic variations of the surface properties can be monitored by STM and photoemission spectroscopy. It is well known that ZnO can be easily sulfidized by H_2S [17] and therefore it is not

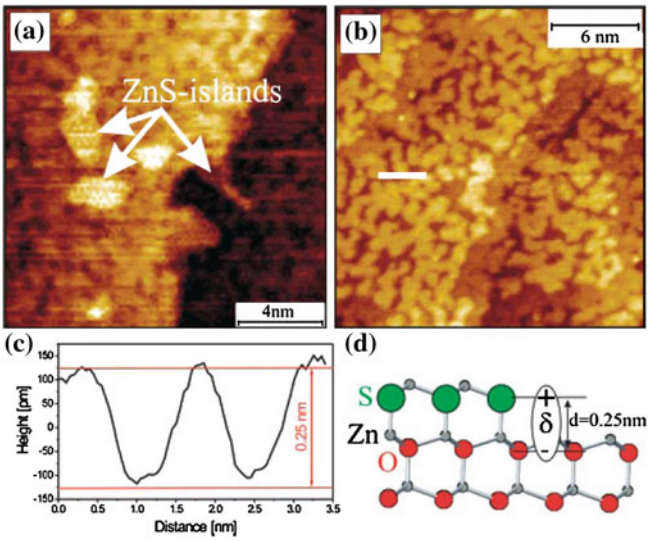

Fig. 2.7 STM images of sulfur induced surface structure for **a** 0.6 L H_2S and **b** 3 L H_2S exposure. The cross-section indicated in (**b**) is shown in (**c**). A ball-and-stick model of the surface structure is shown in (**d**) with the surface dipole moment indicated. Reprinted with permission from Ref. [18]. Copyright 2008, American Chemical Society

surprising that a ZnO sample held at 400 °C and exposed to H_2S converts to ZnS. STM studies show that two dimensional ZnS islands form at the surface of ZnO and these islands grow with exposure until the surface is covered with a dense network of meandering ZnS islands [18]. This is shown in Fig. 2.7. Although the atomic scale structure of the sulfide film cannot be unambiguously deduced from these STM studies, some islands exhibit hexagonal symmetry. Consequently, it is reasonable to assume that ZnS adopts the wurtzite structure of the ZnO substrate and an epitaxial relationship between substrate and film is established. The much larger lattice constant of wurtzite-ZnS ($a = 3.82$ Å; $c = 6.26$ Å) compared to ZnO ($a = 3.25$ Å; $c = 5.21$ Å) implies that a complete ZnS monolayer would be under considerable compressive stress. The formation of ZnS island morphology provides an efficient strain relieve mechanism for pseudomorphic ZnS layers. Thus STM allows a direct observation of the transformation of the surface of a gas-sensing material during the reaction with the environment. This real space information of the surface morphology is important for correctly interpreting spectroscopic information. Soft x-ray and ultraviolet photoemission enable monitoring the compositional and electronic-structure variation as a function of H_2S exposure and this can be correlated to the morphology changes measured by STM. The band bending, which is measured in photoemission spectroscopy by evaluating the core-level position shifts relative to the Fermi-level, is a direct measure of the gas response of the semiconducting metal oxide. Therefore the gas response

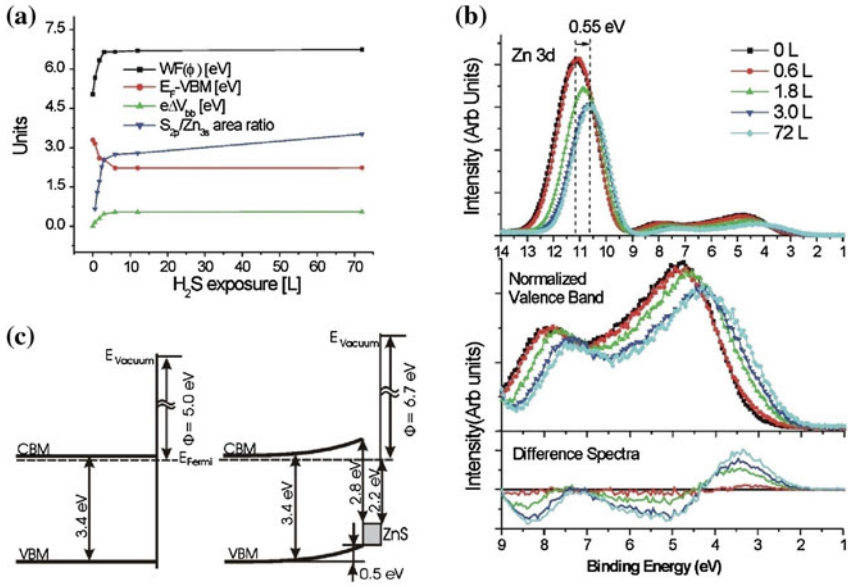

Fig. 2.8 Information obtained from photoemission spectroscopy on the surface response of ZnO to reaction with H_2S. **a** Summary of the changes in the work function, valence band maximum (relative to the Fermi level), band bending in the substrate, and the S 2p/Zn 3s peak ratios as a function of H_2S exposure. **b** Valence band and shallow Zn-3d core level spectra for different H_2S exposures. The shift in the Zn-3d core-level represents the band bending. The change in the valence band is shown in bottom panel of (**b**). The difference spectra are calculated by subtraction of the spectrum of the clean surface after shifting it to compensate for band bending effects. Therefore the positive intensity correspond to electronic states formed by ZnS formation. These electronic structure information are summarized in the band diagram displayed in (**c**). Reprinted with permission from Ref. [18]. Copyright 2008, American Chemical Society

can be measured in photoemission without directly detecting changes in the material conductivity.

Information extracted from photoemission studies of ZnO surface exposed to H_2S is summarized in Fig. 2.8a [18]. Together with STM this gives a comprehensive representation of the processes and changes of a gas sensing surface during operation. It is apparent from Fig. 2.8a that within the first 4 L (Langmuirs) of exposure most of the surface changes causing the gas sensing response have already taken place. The sulfur uptake measured by the S-2*p*/Zn-3*s* core-level ratio is rapid for the first 4 L and only very gradually increases at higher exposures. This is consistent with a 2D mono-layer growth of ZnS observed in STM. Photoemission suggests that further sulfidation upon completion of the monolayer is slow and all the gas sensing action can be attributed to the monolayer formation as evidenced by the band bending that occurs simultaneously with the initial sulfur uptake. Since photoemission is a surface sensitive technique, it detects electrostatic binding energy shifts in the Debye layer which in semiconducting oxides is much larger than the probing depths in photoemission. In the case of sulfide formation on

ZnO(0001)-Zn surface, 0.5 eV upward band bending is observed after exposure to 4 L H_2S.

In addition, valence band spectra reveal that, although ZnS is a wide band gap material, additional electronic states are formed within the band gap of ZnO. The change in the valence band is shown in Fig. 2.8b and the decrease in the separation between the valence band maximum (VBM) and the Fermi-level is also indicated in Fig. 2.8a. Finally, the work function change can be evaluated from the secondary electron cut-off in photoemission experiments. These measurements indicate that the work-function of the sample increases quite strongly upon sulfidation of the surface. This change in the work function is attributed to formation of a surface dipole as illustrated in Fig. 2.7d.

Measurement of band bending, work function, and valence band enables derivation of the surface electronic structure for a sulfidized surface. This is shown in Fig. 2.8c. Obviously the 0.5 eV upward band bending would give rise to a decrease in conductivity and thus this is the main reason for the gas response of ZnO towards H_2S. In other studies it has been shown that sulfidation can be reversed by oxidation and therefore in the absence of H_2S the pure ZnO surface can be re-established in air. The reversibility of the surface composition makes this a good sensing process.

This example of the sulfidation of ZnO by H_2S exposure illustrates how surface science can be used to measure the fundamental surface transformations responsible for the gas response by surface reactions. Because these studies are performed under UHV conditions the surfaces are only exposed to one gas. In real gas sensing applications the H_2S would be a trace amount in e.g. air. Therefore it would be interesting to investigate the role of other gases on the surface changes. Advances in 'high pressure' photoemission experimental set-ups [19], which become now more common at synchrotron facilities, will enable to do surface science experiments under more realistic pressure and gas mixture conditions in the near future and thus enable us to close the 'pressure gap' between fundamental surface science studies and 'real world' conditions. Although there have been several studies on heterogeneous catalyst surfaces [19] and even on solid-oxide electrochemical cells under operating conditions [20], there are, to the best of our knowledge, no ambient pressure studies on gas sensor surfaces been reported yet. Ambient pressure XPS studies would enable us to monitor surface properties under different chemical potentials of the gas phase and thus circumvent the inherent problem of UHV surface science studies of investigating surfaces in an unrealistically strong reducing environment.

2.3 TiO_2 Studies

Titanium dioxide is often used as a model system for transition metal oxide surfaces [21]. Consequently, the surface properties of TiO_2 are the best understood of all oxides. TiO_2 exists in three different crystal structures: rutile, anatase and

brookite. Of those three, only rutile and anatase are of technological importance. Rutile is thermodynamically the most stable polymorph, however, for nanomaterials anatase may become favored. Most surface studies have been performed on rutile, because of the commercial availability of single crystal samples. Experimental studies on anatase have either been performed on mineral samples or on epitaxial thin films grown on $SrTiO_3$ or $LaAlO_3$ substrates [22, 23]. In here we are focusing on the rutile phase of TiO_2.

Transition metal oxides may sense reducing and oxidizing gases due to formation and reaction with charged surface species, namely O_2^- and O^- radicals [2], or due to the reaction of lattice oxygen, i.e. bulk reduction. The former detection mechanism is dominant on materials whose conductivity may be strongly affected by charged adsorbates induced band bending such as SnO_2, ZnO or In_2O_3. The conductivity of TiO_2 on the other hand is more strongly affected by bulk reduction and oxidation. Nevertheless, the well ordered surfaces of TiO_2 make it an ideal model system for studying fundamental aspects of single molecule chemistry by e.g. STM. A review of such atomic-scale studies may be found in [24] for studies on the rutile (110) surface. The (110) surface is by far the most extensively studied surface orientation of rutile and most important properties of this surface are reviewed in [21]. Another prominent surface of rutile TiO_2 is the (011) orientation, which is the second most abundant surface in the Wulff equilibrium crystal shape construction of rutile. The (011) surface has obtained far less interest in the fundamental surface science community. The very different structural properties of the (110) and (011) surface, however, enable a nice comparison of the influence of surface structure on the surface chemical properties and thus chemical sensing behavior. Therefore in the next section we will discuss these differences.

The importance of the surface structure leads to the question on how the structure can be modified in order to achieve better selectivity and sensitivity towards target gases. Although its effectiveness for tuning gas responses is still unproven, a new ion beam method is described that enables fabrication of unique step edge structures on planar metal oxide surfaces. Finally, we end the discussion of TiO_2 by investigating the re-oxidation of TiO_2(011) crystals. This is the important process of changing the intrinsic dopant concentration and thus underlies the gas response mechanism for oxidizing and reducing gases of TiO_2.

2.3.1 Comparison of the Rutile-TiO_2 (011) and (110) Surfaces

The surface structure of stoichiometric TiO_2(110) is a bulk truncation with only small atomic relaxations. Figure 2.9a shows a model of the surface structure of TiO_2(110). The (110) surface exhibits two-fold coordinated bridging oxygen atoms that protrude from the surface plane and are closely spaced (0.30 nm) along the [001] direction and are far apart (0.65 nm) along the [10] direction. This gives the surface a large corrugation and a strong structural anisotropy. Slight reduction of TiO_2 by vacuum annealing, causes the removal of $\sim$10 % of the bridging

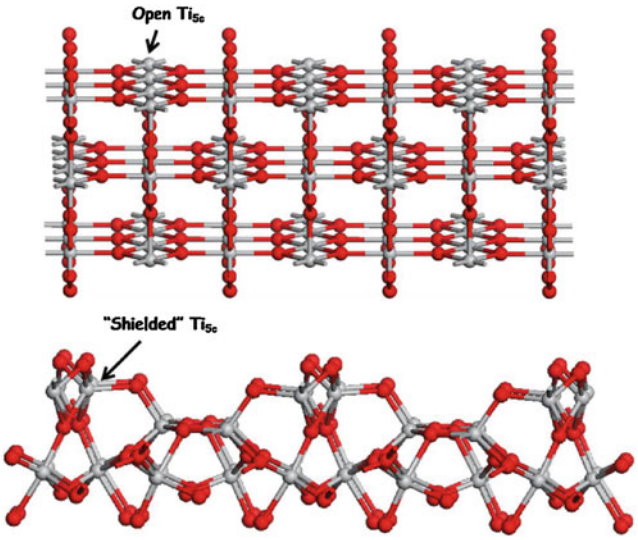

Fig. 2.9 Ball-and-stick models for TiO_2(110) (**a**) and (011)-2 × 1 (**b**) surfaces. *Grey* and *red* spheres are Ti and O atoms, respectively

oxygen atoms, i.e. formation of oxygen vacancies. These vacancies are very reactive surface sites and even under UHV conditions are quickly filled by adsorption of residual water from the gas phase. Water adsorbs dissociatively in these O-vacancy sites leaving two hydroxyls at the surface. This adsorption of water at defects has been studied extensively by STM [24]. Because of the very high reactivity of O-vacancies their relevance for realistic environmental conditions is doubtful. Reduction by vacuum annealing does not only induce surface O-vacancies but it also increases the number of bulk Ti-interstitials. This formation of interstitials can be reversed by annealing in an oxygen atmosphere which is discussed below.

Unlike the (110) surface, the rutile TiO_2(011) surface reconstructs to form a 2 × 1 periodicity. The structure of this surface reconstruction was recently resolved by surface x-ray diffraction measurements and density functional theory (DFT) calculations by two groups independently [25, 26]. The proposed structure is shown in Fig. 2.9b. This surface exhibits two different surface Ti_{5c} atoms, with each of them coordinated to 2-fold coordinated oxygen (O_{2c}) atoms that protrude out of the surface and partially 'block' the Ti_{5c} atoms from the gas phase and thus potentially hindering molecular adsorption. Although the density of Ti_{5c} at the (011)-2 × 1 surface is slightly higher than on the (110) surface (0.08/Å^2 compared to 0.05/Å^2), the closest separation between Ti_{5c} is similar on the (110) surface (2.959 Å) and on the (011)-2 × 1 surface (2.963 Å). However, these closest separated Ti_{5c} atoms on (011)-2 × 1 are coordinated to bridging two fold coordinated O_{2c} atoms while on the (110) surface the Ti_{5c} sites are 'open' to the gas phase as is apparent in Fig. 2.9. Consequently, the large structural differences

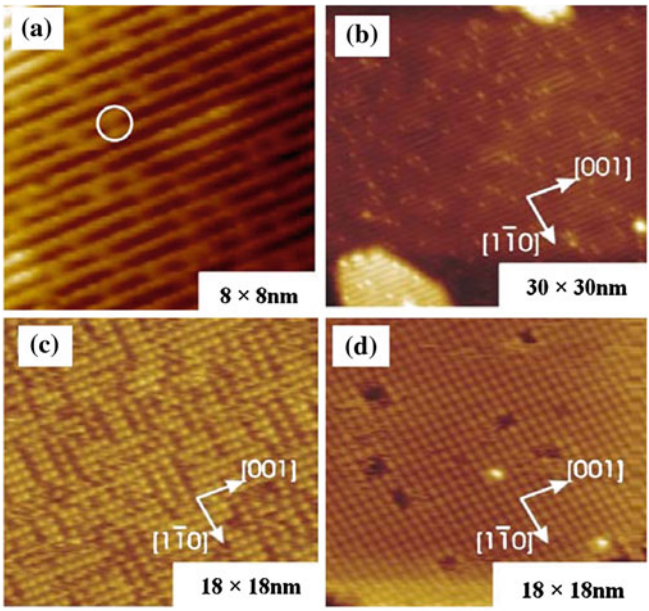

Fig. 2.10 STM images of acetic acid adsorption on TiO_2(110). **a** clean, vacuum-prepared TiO_2(110) (8 × 8 nm^2). **b** and **c** after adsorption of 0.16 and 0.43 acetate, respectively. And (**d**) close to saturation coverage of 0.5 ML forming an ordered 2 × 1 over layer structure. Reprinted with permission from Ref. [34]. Copyright 2011, American Chemical Society

between these two surfaces suggest different adsorption properties. One example of the largely different adsorption is discussed below on the example of acetic acid adsorption. Now that the surface structure of the (011) surface is resolved, we may expect more studies on the surface chemistry of this surface in the near future.

STM images of vacuum-annealed TiO_2(110) and (011)-2 × 1 surfaces are shown in Figs. 2.10a and 2.11a, respectively. The bright and dark rows in Fig. 2.10a correspond to surface five-fold Ti atoms (Ti_{5c}) and two-fold bridging oxygen (O_b) sites, respectively [21]. There are several bright spots between the bright rows which are attributed to surface bridging O vacancies (O_b-vac) or -OH, where the latter is formed by water dissociation at O_b-vac sites, as is typical for this surface. In contrast to TiO_2(110), the STM image of clean TiO_2(011)-2 × 1 surface exhibits rows of protrusions arranged in zigzag patterns as given in Fig. 2.11a. The bright spots in the STM image have been attributed to the geometrically protruding two-fold O (O_{2c}) atoms arranged in a zigzag pattern along the [100] direction (see Fig. 2.9b) [27].

Initial studies of water [26] and carboxylic acid [28] adsorption suggest that the (011)-2 × 1 surface behaves very different compared to the (110) surface. Strongly different molecular interaction with surfaces of different atomic

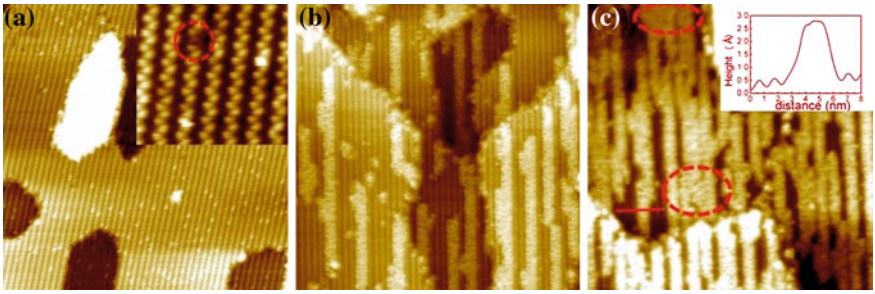

Fig. 2.11 STM images of acetic acid adsorption on TiO_2(011)-2 × 1. **a** clean vacuum prepared surface. **b** and **c** after exposure of 18 and 24 L acetic acid, respectively. Reprinted with permission from Ref. [34]. Copyright 2011, American Chemical Society

arrangements and coordination suggest face dependent gas responses in gas sensing materials. In the next section we investigate the role the surface structure plays for molecular adsorption on the example of acetic acid adsorption.

2.3.2 *Comparative Study of Acetic Acid Adsorption on TiO_2(110) vs. (011)-2 × 1*

The adsorption of carboxylic acid on TiO_2(110) was extensively investigated by STM, photoemission spectroscopy (PES) [29–31], and computational methods [32]. The 'open' rows of closely spaced Ti_{5c} cations are ideal sites for carboxylic acids to adsorb dissociatively by splitting-off its acidic hydrogen (which adsorbs on the surface lattice oxygen). The lattice spacing is such that the acetate adsorbs in a bidentate fashion, bridging two neighboring surface Ti_{5c} [33]. On the TiO_2(011)-2 × 1 surface, on the other hand, the O_{2c} are bridging the nearest Ti_{5c} atoms preventing a bridge bidentate adsorption of acetate.

Figure 2.10 shows STM images for various stages of acetic acid adsorption on TiO_2(110) at room temperature. The vacuum-annealed clean surface is shown in Fig. 2.10a. The bright and dark rows correspond to surface Ti^{4+} and bridging O^{2-} sites, respectively [20]. Figure 2.10b, c and d show the TiO_2(110) surface with increasing amounts of acetic acid coverage. Adsorbed acetate appears in the STM images as bright spots on top of the Ti_{5c} rows. At room temperature these individual acetate molecules are mobile and subsequent images of the same area show the acetate at different positions along the Ti_{5c} rows. The mobility and diffusion of acetate on this surface has been studied by Onishi and Iwasawa [33]. Also it is worth pointing out that at this low coverage the acetate never comes very close to each other indicating a repulsive interaction between individual acetates along the Ti_{5c} rows. With increasing acetic acid exposure the density of the adsorbed acetate increases. In Fig. 2.10c the surface is covered with ~0.43 $ML_{(110)}$ acetate. At this coverage different domains with ordered superstructures are observed. The

formation of these structures can be understood from the repulsive interactions along the [001] direction, i.e. along the Ti_{5c} rows, which causes the acetates to maximize their separation in this direction, and an attractive force for acetates perpendicular to the Ti_{5c} rows, i.e. in the $[1\bar{1}0]$ direction. This latter explains why acetates preferentially form next-neighbor configurations in the $[1\bar{1}0]$ direction [33]. At saturation coverage, shown in Fig. 2.10d, the acetate over layer arranges in a 2 × 1 superstructure with 0.5 $ML_{(110)}$ coverage.

The well established adsorption of acetate on the TiO_2(110) surface is contrasted to that on the less studied TiO_2(011)-2 × 1 surface [34]. STM images of the clean TiO_2(011)-2 × 1 surface show rows of protrusions arranged in zigzag patterns, as can be seen in Fig. 2.11a. Compared to the TiO_2(110) surface these Ti_{5c} atoms are less accessible because they are coordinated to the protruding O_{2c} atoms. Consequently, the O_{2c} atoms may 'block' the adsorption of acetic acid or form a kinetic barrier for adsorption of acetate to the Ti_{5c} sites on this surface. Indeed, STM images of acetate adsorbed on the (011)-2 × 1 surface shows a very different adsorption behavior compared to the (110) surface. Figure 2.11b shows an STM image taken after a nominal acetic acid exposure of 18 L. Contrary to the homogenous acetate adsorption on the TiO_2(110) surface, acetate clusters appear on the (011)-2 × 1 surface. Initial adsorption of acetate on the (011)-2 × 1 surface is limited to surface defects, such as step edges and antiphase domain boundaries in the 2 × 1 surface reconstruction. This indicates that acetates do not adsorb on perfect defect free (011)-2 × 1 surface under vacuum conditions at room temperature. Defect sites are needed to form nuclei of acetate islands that then can grow onto the defect free terraces. This indicates that the adsorbed acetates in the cluster facilitate further adsorption of acetic acid molecules to the edges of the cluster. Also, the clusters form one dimensional (1D) chains along the $[0\bar{1}1]$ direction, suggesting that diffusion of individual acetates along those rows is the preferential diffusion direction and/or the acetic acid molecules preferentially attach to this side of the clusters only. With increasing acetic acid exposure, the acetate clusters grow in length and the density of the cluster increases until about 77 % of the surface is covered. An STM image of this 'saturation' coverage is shown in Fig. 2.11c for a nominal acetic acid exposure of 24 L. Even much higher doses do not increase the surface coverage significantly anymore, probably because of the lack of sites for acetic acid to attach to the existing acetate clusters. The absolute number of this 'saturation-coverage' may however sensitively depend on the initial defect concentration on the surface. At high coverage many acetate chain-islands merge as indicated by the dashed circles in Fig. 2.11c. As shown in the inset of the Fig. 2.11c, the line profile shows that the 1D cluster chain has corrugation of ∼2.5 Å. The quasi-1D clusters predominantly consist of three lines of bright protrusions that are assigned to adsorbed acetates. The protrusions in the center of these clusters align with the 'dark' rows of the substrate and the protrusions to the left and right are situated over the zigzag rows of the substrate. Furthermore, the center row is always imaged brighter in STM with an apparent height difference between the centre and outer rows of ∼0.3 Å. Because of tip

convolution effects the width of these clusters is overestimated in STM images. From analysis of clusters with a larger width and correlation of the protrusions with the periodicity of the substrate it was concluded that the width of the three-row clusters corresponds to the width of a 2 × 1 substrate unit cell. The acetate ions on the left and right rows are shifted in $[0\bar{1}1]$ direction by half a substrate unit cell, indicating that they are bonded to the lattice Ti_{5c} in the zigzag pattern. Besides the well ordered three-row structure, most of the clusters exhibit a high density of acetate 'vacancies'. Most of these vacancies are located in the two outer rows. For a densely packed cluster we count three protrusions per 2 × 1 substrate unit cell, i.e. 1.5 $ML_{(011)}$ equivalent or 6.0 molecules/nm^2.

In conclusion, these STM studies indicate a quite different acetate adsorption on these two TiO_2 surfaces. While on the TiO_2(110) surface acetate adsorbs readily, acetic acid does not seem to adsorb dissociatively on the perfect TiO_2(011)-2 × 1 surface and initial adsorption is limited to defect sites at room temperature. This suggests a low initial sticking coefficient of acetic acid on the (011)-2 × 1 surface. However, once acetate clusters have nucleated at defects the experiments show that clusters grow and eventually cover large portions of the substrate. Thus the adsorption structure and kinetics is very different on these two surfaces. Further differences in the charge transfer between the TiO_2 substrate and the adsorbed acetic acid can be detected in UPS measurements. In these studies defect states induced by electron donation to the TiO_2 substrate mainly from adsorbed hydrogen plays an important role. This is introduced first before we turn to the charge transfer induced by dissociative acetic acid adsorption.

2.3.2.1 Defect and Adsorbate Induced Band-Gap States in TiO_2

Excess-charge induced Ti-3*d* states within the band gap of TiO_2 have been studied extensively on the (110) surface. These excess charges can originate from surface oxygen vacancies O_{vac} [35], which introduces two excess electrons, or adsorbed hydrogen [36], which introduces one excess electron. These excess charges are transferred to the Ti-3*d* states, which has been verified by resonant photoemission studies [37, 38]. The occupied Ti-3d states are observed in ultraviolet photoemission spectroscopy (UPS) [35], as a band-gap state (BGS) about 0.9 eV below the Fermi level (E_F) for the (110) surface.

Figure 2.12a and b compare the differences between the defect states on (110) and (011) surface for vacuum prepared samples. In Fig. 2.12a, besides the main feature of predominantly O 2*p* derived valence band states of bulk TiO_2(110), the Ti-3*d* derived band gap state (BGS) (located ∼0.9 eV below E_F) is clearly observed. On the vacuum prepared (011)-2 × 1 surface, on the other hand, the BGS is very small (see Fig. 2.12b). The BGS intensities are 1.9 and 0.17 % of the total valence band intensity for the (110) and (011) surfaces, respectively. This is consistent with STM observations of fewer point-defects on the (011)-2 × 1 surface compared to the (110) surface, which have been counted in STM images to

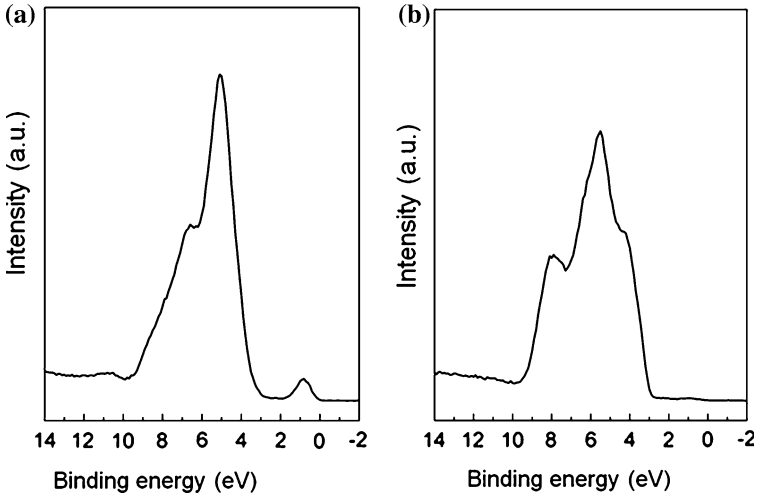

Fig. 2.12 UPS spectra of vacuum prepared rutile surfaces: **a** TiO_2(110) and **b** (011)-2 × 1. Reprinted with permission from Ref [41]. Copyright 2010, American Chemical Society

typically amount to ∼10 % and ∼1 % for (110) and (011)-2 × 1 surfaces, respectively. Therefore the BGS intensity ratio in UPS agrees with the point-defect density on these two surfaces.

2.3.2.2 UPS Measurements of Acetic Acid Adsorption

To investigate the effect adsorbates may have on the defect states, acetic acid has been adsorbed on the two surfaces and the change in the electronic structure measured by UPS. The UPS spectra for (110) surface before and after acetate adsorption is shown in Fig. 2.13a. As shown by the difference spectrum in the lower panel of Fig. 2.13a, the acetate orbitals are mainly located at binding energies of ∼10.4, ∼8.1 and ∼5.7 eV, which agrees for example with the reported values for bi-dentate adsorbed acetate on Cu(110) surfaces [39]. The higher binding energy peaks are dominated by the methylic carbon and carboxylic carbon orbitals while the low binding energy peak originates from carboxylic oxygen atoms, which have direct bonding with the substrate through the oxygen lone pair [39, 40]. In addition to the acetate molecules, contributions from OH_σ are expected. However, the binding energy of the OH_σ bond overlaps with the acetate peak at ∼10.4 eV and therefore OH formation cannot be unambiguously confirmed from the UPS spectra.

Interestingly the UPS studies show that although the adsorbed hydrogen donates its electron to the substrate, the BGS on the (110) surface is decreased by ∼40 % upon carboxylic acid adsorption. This indicates that on the (110) surface, the adsorbed acetate is taking up the charges donated from the hydroxyls—formed

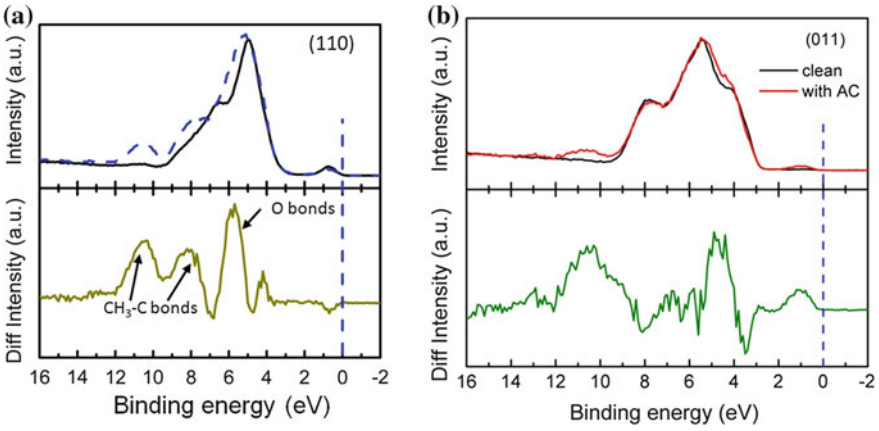

Fig. 2.13 UPS valence band spectra of **a** TiO_2(110) and **b** TiO_2(011)-2 × 1 before (*black solid curve*) and after monolayer acetate adsorption (*blue/red curves*). The difference spectra between the clean and acetate covered surfaces are shown in the lower panels. The defect states just below the Fermi-level (0 eV binding energy), behaves oppositely on the two surfaces. On the (110) surface the defect state decreases while on the (011)-2 × 1 surface the defect state increases upon acetic acid adsorption. Reprinted with permission from Ref [41]. Copyright 2010, American Chemical Society

by the dissociative adsorption of acetic acid—and even reduces the excess charges in the sample that were present prior to acetic acid adsorption. This contrasts observations on the (011)-2 × 1 surface. Adsorption of acetic acid on TiO_2(011)-2 × 1 at room temperature also results in dissociative adsorption. However, contrary to the (110) surface, the BGS is increasing on the (011)-2 × 1 surface upon acetate adsorption, as shown in Fig. 2.13b. This implies that the acetate is not able to take up all the excess charges donated by the hydroxyls, leaving charges in Ti-3*d* states. This difference may originate from the adsorption coordination of the acetate with a monodentate vs bidentate adsorption on the (011)-2 × 1 and (110) surface, respectively. Having two acetate-oxygen atoms coordinated to the (110) surface enables acetate-molecules to overcompensate for the electrons donated by hydroxyl formation and consequently resulting in the observed suppression of the BGS. In contrast, coordination of only one oxygen atom of the acetate to the substrate on the (011)-2 × 1 surface leaves excess charges (donated by –OH groups) in the TiO_2 substrate. Understanding the differences in charge transfer from the metal oxide to the adsorbate has important implications for gas sensing mechanisms, since the surface charge are largely responsible for the gas response in conductivity sensing materials. Therefore, as more crystallographically defined gas sensing materials are being developed; surface science studies of face-dependent charge transfer mechanisms can provide answers to fundamental gas sensing mechanisms.

In addition to the change in intensity of the BGS for the two surfaces a difference in the binding energy for the two surfaces was also observed. Comparing

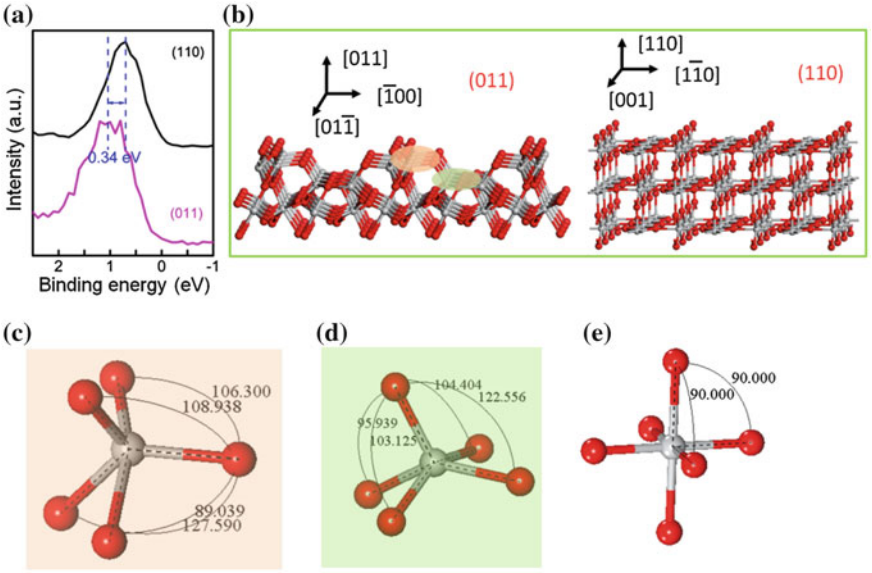

Fig. 2.14 **a** The BGS for the TiO_2(110) and (011)-2 × 1 surfaces are compared. The *black curve* is for the clean TiO_2(110) surface and the *pink curve* is measured on the (011)-2 × 1 surface after acetate adsorption, when the BGS becomes noticeable. The BGS for the (011) surface is shifted ~0.34 eV to higher binding energies compared to the (110) surface. **b** *Ball*-and-*stick* models for TiO_2(011)-2 × 1 and (110) surfaces. Grey and red spheres are Ti and O atoms, respectively. **c** and **d** show two different local Ti–O environments on the (011)-2 × 1 surface with the same color code specified in (**b**). **e** shows the octahedral coordination environment for bulk TiO_2. The values shown in (**c**), (**d**) and (**e**) are the bond angles

the BGS binding energy for the (110) and (011)-2 × 1 surface reveals that the binding energy of the BGS for the (011)-2 × 1 surface is ~ 0.34 eV higher than for the (110) surface, as emphasized in Fig. 2.14a. This is a significant energy difference for excess charges at Ti lattice sites and suggests that electrons are more effectively trapped on the (011)-2 × 1 surface than on the (110) surface.

This higher binding energy of Ti-3*d* states on the (011)-2 × 1 surface has been explained by the geometry of the surface reconstruction and the resulting crystal field at the surface Ti-sites [41]. Due to the surface reconstruction, the Ti–O coordination environment at (011)-2 × 1 surface is changed to two differently distorted square pyramid Ti–O coordination as schematically shown in Figs. 2.14c, d. Generally, a square pyramid coordination causes a larger crystal field splitting and stronger stabilization of the d_{xz} and d_{yz} orbitals compared to an octahedral configuration. Only Ti-atoms in the topmost surface layer exhibit this unique coordination environment and therefore the observed higher binding energy of the Ti-3*d* state implies that the defect-electrons are localized in the surface layer.

2.3.3 Surface Modification by Grazing Incidence Low Energy Ion Sputtering

In the previous section it has been shown that surface structures and defects play an important role in the adsorption of molecules and thus in the gas sensitivity of these materials. Therefore, it would be important to be able to modify surface structures to enable tuning of surface sensitivity to specific target gases. This requires a surface modification at the molecular scale since this is the relevant length scale for adsorption. On oxide surfaces, under-coordinated sites can be particularly reactive. Such sites are, for instance, step edges. Consequently, creating surfaces with a high density of defined step edge structures may be an approach for tuning gas sensitivities of materials. In the following we describe a method that enables such a surface structuring on the example of TiO_2(110). This method employs grazing incidence low energy ion beams and exploits a self organization of the surface into nano-ripple structures that exhibit a high density of step edges.

It has been demonstrated that the sputter yield of a grazing incidence low energy ion beam varies largely at flat terraces compared to defect sites such as step edges [42, 43]. Thus, ion sputtering at grazing angles is fundamentally different from sputtering at steeper angles. At steeper angles, the ions deposit their energy in the bulk. At grazing angles, on the other hand, planar surfaces re-arrange to minimize step-edge sputtering. This results in an alignment of step edges in the direction of the azimuth direction of the ion beam. The alignment of step-edges combined with a sputter induced surface roughening gives rise to the formation of nanoscale ripples at the surface. This process is discussed next followed by a demonstration that this ion beam techniques also allows the formation of high energy step edge orientations that otherwise cannot be observed.

2.3.3.1 Nanoripple Formation by Grazing Ion Sputtering

Grazing incidence sputtering by low-energy ions can be applied to many planar single crystal substrates. With increasing ion-incident angle (measured from the surface normal) the sputter yield initially increases because the ion energy is deposited closer to the surface and thus collision cascades cause the ejection of more surface atoms. However, at a critical grazing incidence angle most of the incident ions will be quasi-elastically reflected from the surface without penetrating the surface. Furthermore, for low energy ions, the momentum transfer to the surface during the reflection is too small to induce lattice defects at defect-free terraces. At surface defects, and in particular at step edges, the incident ions can, however, interact more strongly with the substrate and thus induce sputter damage at these pre-existing surface defects. This results in a sputter yield that varies locally on the surface and this gives rise to a self-organization of the surface in nanostructures.

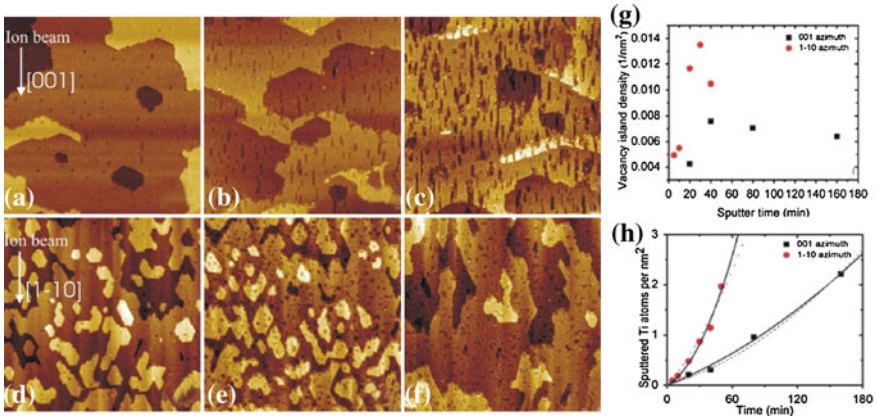

Fig. 2.15 Shown are 200 × 200 nm STM images of TiO_2(110) after grazing incidence irradiation along the <001>azimuth for **a** 20 min, **b** 80 min, and **c** 160 min, and along the <10> azimuth for **d** 5 min, **e** 20 min, and **f** 30 min. **g** shows the evolution of the vacancy island density with sputter time. The totaled sputtered atoms derived from the total vacancy island area as a function of sputter time is shown in (**h**). Reprinted from Ref. [44]. Copyright 2010, American Physical Society

The initial surface evolution, i.e. for low ion fluences, is shown in Fig. 2.15 for two different ion beam azimuths at 8° grazing incidence angle. In the low fluence regime the ion beam induced formation of vacancy islands and their gradual evolution into vacancy islands with an elongation along the ion beam azimuth can be observed. Formation of vacancy islands is due to random terrace sputtering of atoms which agglomerate by surface diffusion into islands at the processing temperature of ∼400 °C. Once the vacancy islands are formed increased sputtering is observed along the step-edges facing the ion beam. This has two consequences; firstly the total sputter yield from the surface increases with an increasing step edge density and secondly the vacancy islands form an anisotropic shape due to the preferential sputtering at step edges exposed to the ion beam. It is apparent from Fig. 2.15 that this mechanism is also dependent on the crystallographic azimuth of the ion beam irradiation. Especially on TiO_2(110) where the surface structure is very anisotropic the sputter yield of a grazing ion beam will also be anisotropic. Furthermore, variations of the step edge formation energies (see below) prefer certain step edge orientations which can favor vacancy islands with distinct shapes.

The total amount of sputtered atoms can be deduced from the surface area covered with vacancy islands that enables a measure of the sputter yield. Figure 2.15g and h plots the vacancy island density and the number of sputtered atoms versus the ion fluence for the two azimuths directions investigated. The non-linear change in sputtered atoms with ion fluence indicates that the sputter yield increases with irradiation time. This can only be explained if the changing surface morphology affects the sputter yield. This is further indication that step

edge sputtering is a crucial component of the total sputter yield. For both azimuths the step edge density increases with sputter time, due to the formation of vacancy islands, and consequently increases the global step edge sputter contribution. As shown in Ref. [44] fitting a quadratic expression to the sputtered atoms vs ion fluence plot and estimating the step edge density from STM-images, the relative contributions from step edge and terrace sputtering can be extracted. This kind of analysis shows that the step edge sputtering is more than ten times that of the terrace sputtering.

With increasing ion fluence the surfaces increase in roughness as the STM images shown in Fig. 2.16 indicate. However, instead of forming a randomly rough surface, nanoripples form. These nanoripples are aligned with ion beam azimuth and thus exhibit mainly step edges that are in the direction of the ion beam. Furthermore, the ripples exhibit a fairly uniform separation of 10–20 nm and a peak-to-valley roughness of $\sim$4 nm. Therefore this technique of grazing ion beams allows the formation of surfaces with step edges with defined crystallographic orientation and high density. This is a new method for modifying surfaces with under-coordinated sites which may be exploited for tuning chemical and gas sensing properties in the future. This method can be employed not only on single crystals but also on thin epitaxial films and thus this may be exploited for new gas sensing materials. In addition, this ion beam method also has the advantage of being capable of forming step edges that are meta-stable, i.e. step edges with high formation energy. Such steps are often the most chemically active step edges and thus preparation of surfaces with a high density of such steps is especially interesting for obtaining surfaces with new chemical functionalities. This is briefly discussed in the next section.

2.3.3.2 Formation of Meta-Stable Step Edge Orientations

Step edges on oxides and other covalent and ionic materials have strong orientation dependent formation energies. This causes the presences of only step edge orientations with the lowest formation energies to be present on a surface in thermodynamic equilibrium. If the step edge formation energies are known the shape of atomic-layer high adislands can be derived from a 2D analogue of the crystal shape Wulff construction where the surface energies are replaced by step edge energies [45]. For a vacuum annealed TiO_2(110) surface only step edges along the [11] and [001] directions are observed but not in the [10] direction, which would be the third low index direction within the (110) surface. The observed step-edge orientations are illustrated in Fig. 2.17. This implies that the latter direction is an energetically unfavorable direction for step edge formation. Can this direction be prepared using the above described grazing ion beam method?

Directing the ion beam along the [10] azimuth indeed results in step edges aligned in this direction and STM allows the determination of the structure of this step edge [46]. Figure 2.18b and e show atomic resolved STM images. It is

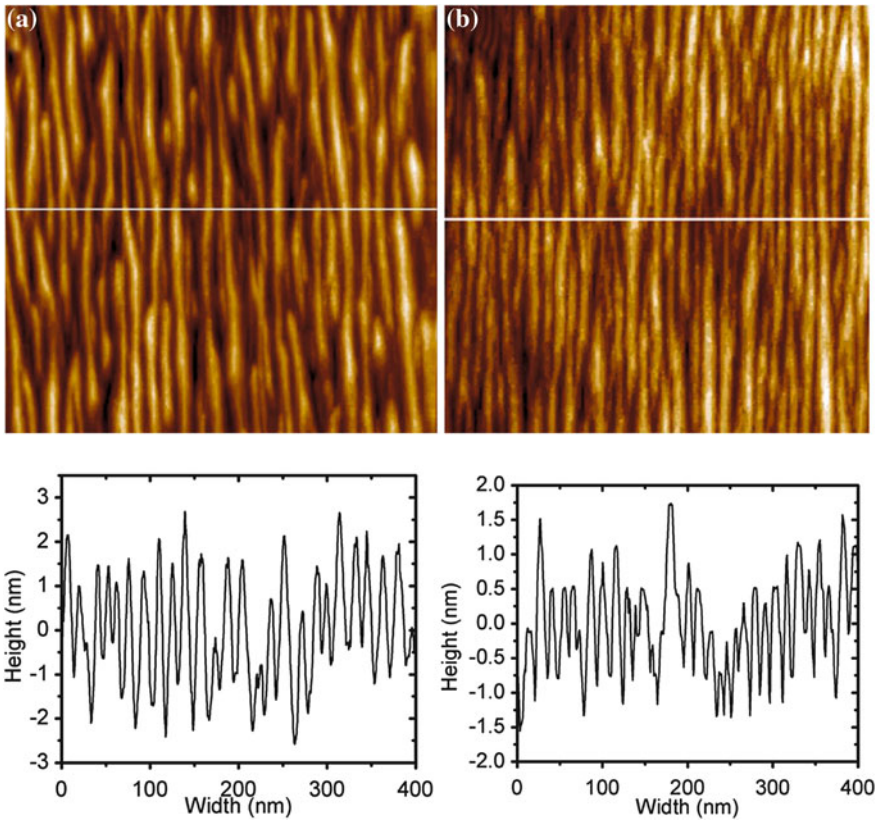

Fig. 2.16 STM images (400 × 400 nm) of the surface morphology after extended periods of grazing incidence irradiation in **a** <110> azimuth- and **b** <001> azimuth-direction. Nano-ripples are formed that are aligned parallel to the ion-beam directions. The corrugation of these ripples is ∼4 nm as can be judged from the shown cross-sections. Reprinted from Ref. [44]. Copyright 2010, American Physical Society

apparent that the periodicity of this step edge is twice that of the terrace. This suggests a step edge structure as shown in Fig. 2.18d and DFT simulations of a STM image of such a step edge results in very good agreement with the measurement. The fact that this step edge is only meta-stable is highlighted by the fact that annealing of the surface to ∼600 °C results in a reformation of energetically more favorable step edges along the [11] azimuths. This is shown in Fig. 2.18c by the formation of zigzagging steps.

In conclusion, the use of grazing ion beam step structuring allows not only the preparation of surfaces with a high step edge density but it also enables the stabilization of steps that are otherwise not present at the surface. Therefore this method may be used to structurally alter the surface and thus tune the sensing properties of metal oxide surfaces.

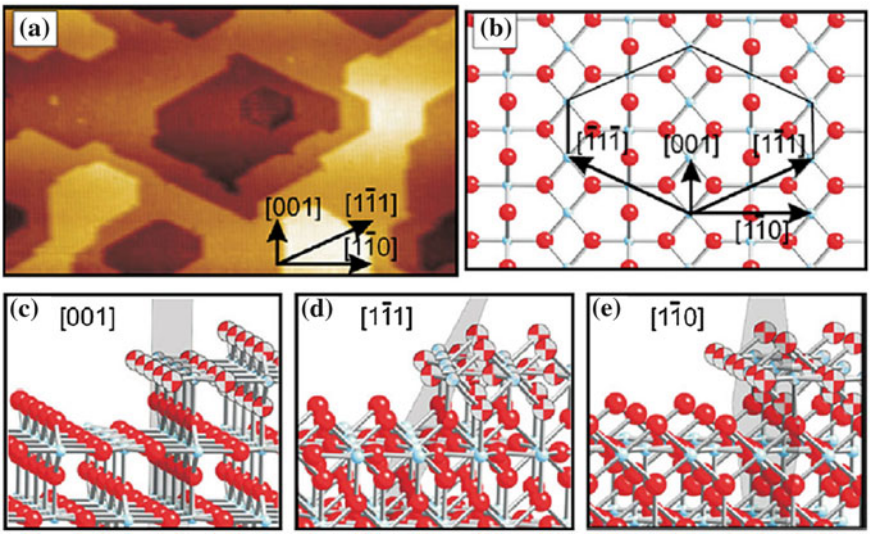

Fig. 2.17 Low energy step-edge structure on TiO_2(110). **a** STM image of a typical surface structure of clean TiO_2(110) surface, **b** orientations of the step edges on the surface (top view), and (**c**)–(**e**) illustrative structures of the different step edges (side views). In (**c**)–(**e**), the shaded area represents micro facets of an extended low index crystallographic plane corresponding to the step edge. Ti and O atoms are represented by small and big balls, respectively. Reprinted from Ref. [46]. Copyright 2009, American Physical Society

2.3.4 Reaction of Sub-Surface Ti Interstitials with Gas Phase Oxygen

When Titania is reduced, excess titanium occupies interstitial sites. These interstitials are fairly mobile and at elevated temperatures can readily diffuse into the bulk. The opposite is also observed. If a reduced TiO_2 crystal is annealed in an oxidizing atmosphere the Ti-interstitials are diffusing to the surface where they can react with oxygen [47, 48]. The formation and annihilation of Ti-interstitials at the surfaces of TiO_2 is directly related to the gas response of TiO_2 to oxidizing and reducing gases. Ti-interstitials act as n-type dopants in TiO_2 and thus changes in their concentration affect the conductivity of the material which can be used as the gas response signal.

The phenomenon of re-oxidation of Ti-interstitials can be directly observed by surface science techniques in vacuum. Annealing of a slightly reduced crystal in $\sim 10^{-6}$ Torr O_2 pressure results in the reaction of Ti-interstitials at the surface with oxygen. As a consequence new layers of TiO_2 are growing at the surface. This has been thoroughly studied on the more frequently investigated rutile TiO_2(110) surface [49, 50]. Recently, the re-oxidation of a slightly reduced TiO_2(011) surface has been studied [51]. Similar to the (110) surfaces oxidation of Ti-interstitials results in the formation of new TiO_2 layers. However, on the (011)

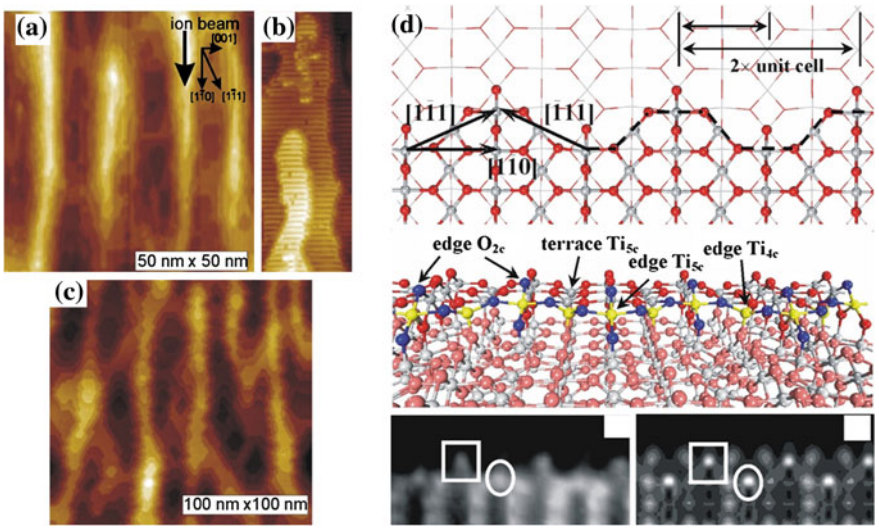

Fig. 2.18 Fabrication of meta-stable step edges by grazing ion beam irradiation along the [10] azimuth of TiO_2(110). (**a**) and (**b**) STM images of surface morphology after grazing ion beam irradiation with the majority of steps aligned with the ion beam azimuth direction along [10]. Annealing to 600 °C results in the restructuring in energetically more favorable [11] steps as evidenced by the zigzagging steps in (**c**). (**d**) shows an atomic scale model of the [10] steps and (**e**) and (**f**) is a comparison of the experimental STM image with a DFT-simulated STM image. Reprinted from Ref. [46]. Copyright 2009, American Physical Society

surface this new TiO_2 surface layer is different in its structural and electronic properties compared to the original surface. This new surface structure and its properties are discussed in the following.

2.3.4.1 Formation of New Metastable Surface Structure on TiO_2(011)

Vacuum prepared clean TiO_2(011) surface undergoes 2 × 1 reconstruction which show rows of protrusions arranged in zigzag patterns in STM images, as discussed above and shown in Figs. 2.9b, 2.19a and b. When this surface is exposed to O_2 at ~300–400 °C, high resolution STM images illustrate that islands with a different structure are formed on the surface as shown in Fig. 2.19c and d. Although the periodicity of the new surface structure can also be described as a (2 × 1) surface unit cell, the structure of these islands is different from the original TiO_2(011)-(2 × 1) surface or a (1 × 1) bulk truncation. In particular, the new surface phase is less corrugated on the atomic scale along the long axis of the surface unit cell than the 'original' surface structure, while having a similar corrugation along the short axis of the unit cell. The corrugation measured in the STM images is shown as the line scan in Fig. 2.19e.

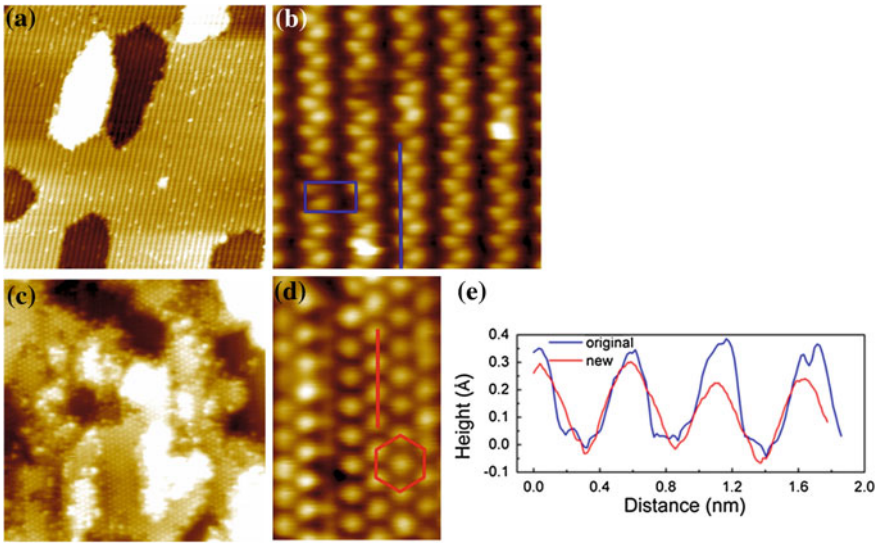

Fig. 2.19 Atomic-resolution STM images of the rutile $TiO_2(011)$ surface. The (2×1) reconstructed surface is shown in (**a**) and (**b**) and the new TiO_2 phase formed after annealing in 10^{-6} Torr O_{2O2} atmosphere is shown in (**c**) and (**d**). The image size for (**a**) and (**c**) are both $(50 \times 50\ nm^2)$. The surface unit cell for the rectangular (2×1) reconstruction is indicated in (**b**) and the quasi-hexagonal symmetry of the new TiO_2 phase is shown in (**d**). A line defect in the new TiO_2 phase can also be seen in (**d**). This defect is an anti-phase boundary due to the registry of the new phase with the $TiO_2(011)$ substrate. The line-profiles indicating the atomic corrugation along the indicated lines in (**b**) and (**d**) are shown in (**e**). Adapted from Ref. [51]

This new surface structure is thermally stable to ~500 °C and only annealing in vacuum above this temperature causes the reformation of the 'original' surface structure. Therefore this new structure is only metastable, however, its fairly high thermal stability suggests that it may be important in applications.

In addition to the structural variation the electronic properties of this new surface structure is also surprisingly different. In Fig. 2.20a and b, scanning tunneling spectroscopy (STS) spectra obtained for the original $TiO_2(011)$-(2×1) surface structure and the new TiO_2 phase are shown. A comparison of STS spectra of the two phases shows that the new phase exhibits filled electronic states that are in the band gap region of bulk rutile TiO_2. Also the empty states exhibit a weak variation between the two surfaces with the conduction band minimum slightly shifted towards the Fermi level for the new phase. Therefore, these spectra demonstrate that the new TiO_2 phase has a smaller band gap than bulk rutile TiO_2.

For a more accurate determination of the filled states of the new TiO_2 structure and to obtain information on the electronic states that make up the new valence band, UPS studies were performed using synchrotron radiation. Figure 2.20c and d show valence band photoemission spectra of the TiO_2 sample. After formation of the new surface structure, a new state within the bulk band gap of TiO_2 is observed with a maximum at 2.1 eV below the Fermi level. From comparison with STS

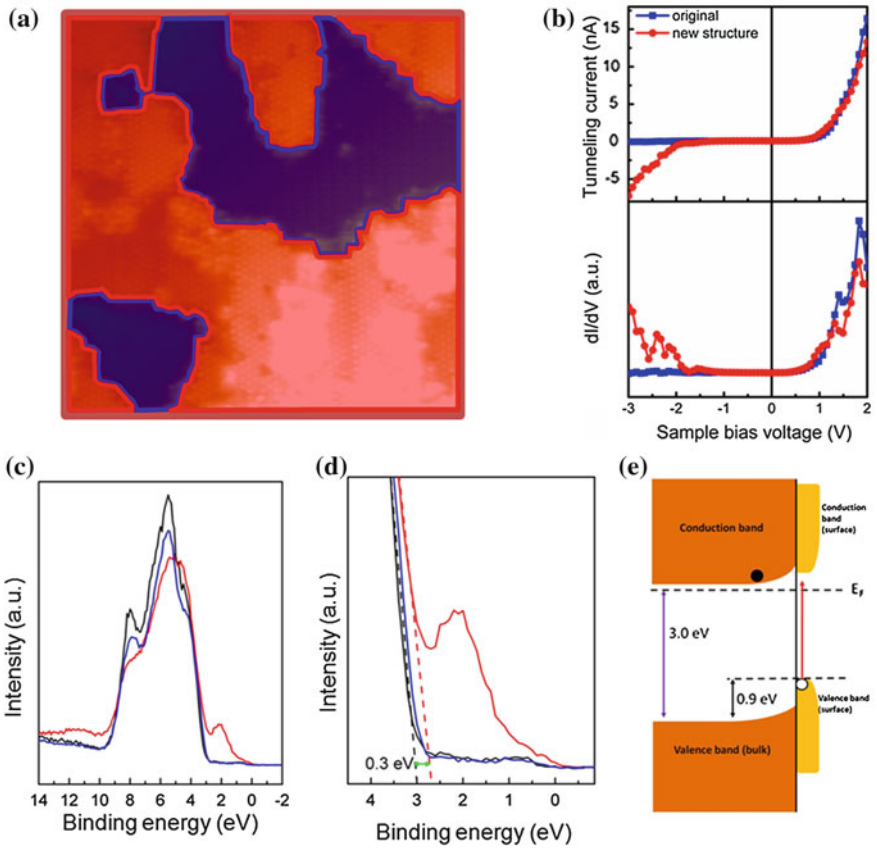

Fig. 2.20 Electronic structure determination of new structure on TiO_2(011) surface. Scanning tunneling spectroscopy (STS) measurements. In (**a**), the original (2 × 1) reconstructed surface is coloured in blue, while the new TiO_2 phase is indicated in *red*. The color coded *I–V* spectra taken in the respective surface areas are shown in (**b**) and the numerically differentiated dI/dV curves are also shown in (**b**). Photoemission spectra confirm the formation of new electronic states within the band gap. UPS spectra taken with an 80 eV photon energy are shown in (**c**) and (**d**). The *black curve* corresponds to the photoemission spectrum for the original (2 × 1) reconstructed surface. The *red curve* has been acquired after low pressure oxidation and (partial) formation of a new TiO_2 phase. The *blue line* indicates a photoemission spectrum that has been taken after annealing the sample to ∼600 °C in vacuum and re-formation of the (2 × 1) surface structure. The band diagram is schematically shown in (**e**). Adapted from Ref. [51]

measurements these filled states are assigned to the new surface phase of TiO_2. After annealing the sample to above 500 °C, the valence band structure of the original TiO_2(011)-(2 × 1) surface is regained (see Fig. 2.20c), demonstrating the reversibility of the structural and electronic surface transformation in agreement with the STM studies. Also, a ∼0.3 eV upward shift of the bulk bands is observed due to band bending at the surface indicating a depletion of the surface regions of charge conduction electrons. Therefore, the formation of this new structure may

aid the gas response not just by oxidation of Ti-interstitials but also by the band bending effect induced by the new surface structure.

Based on the experimental results, the electronic structure energy diagram for this new surface phase can be drawn as shown in Fig. 2.20e. The new electronic state penetrates into the bulk band gap and reduces the surface band gap by 0.9 eV. This observation of the formation of a new surface structure with unique electronic properties illustrates that oxide surfaces, although often considered as static, may exhibit a surprising variability and that their remains many unknowns about their atomic scale behavior especially if in contact with different gas phases. Therefore, oxide surfaces will remain a challenging topic for fundamental surface science studies for some time to come. The better understanding of structural, chemical, and electronic properties of these surfaces will ultimately aid the understanding and tuning of metal oxide gas sensors.

2.4 Summary and Perspective

This chapter has given examples of how surface studies of metal gas sensing materials can add to our fundamental understanding of the gas response of semiconducting metal oxides. We intended to show that surfaces can behave quite differently not just between different materials but also for different surface orientations of the same material and even the same surface orientation under different oxidation potentials. In addition, minority sites, like surface defects, can be crucial in determining the surface reactivity and may play a dominant role in the adsorption of molecules and consequently in the gas response of metal oxides. Therefore, from a surface science perspective, an increase in selectivity and sensitivity may be obtained by designing materials with single surface orientations [52] and by controlling defect constellations by e.g. doping or step edge orientations. For the latter point a method has been described that may be used for designing surfaces with defined step edge orientations and this may provide a way forward, at least for fundamental studies, to examine the role of step edges on gas responses. With the progress in real space analysis of surfaces by STM and other scanning probe techniques we may see more studies of the role of molecular scale surface features on chemical surface properties in the future.

Another important advancement in the surface science of gas sensing materials will be to investigate surfaces under more relevant environments with similar precision as is currently possible by traditional vacuum technology. To achieve this goal some of the surface science techniques that rely on vacuum need to be sacrificed but others will substitute for them and some can be modified to allow for higher pressure conditions. We are at the brink of getting out of vacuum and therefore we may expect to learn a big deal more from surface science studies about the fundamentals of gas sensing in the near future. In particular photoemission experiments can now be performed at elevated pressures [19] at a few selected beamlines at synchrotron facilities around the world. The merger of

vacuum surface science with ambient pressure characterization of surfaces will ultimately enable us to determine what surface processes are central for the gas response.

Acknowledgments Support from the National Science Foundation under grant CHE-0840547 is acknowledged.

References

1. Göpel W (1985) Chemisorption and charge transfer at ionic semiconductor surfaces: implications in designing gas sensors. Prog Surf Sci 20:9
2. Batzill M, Diebold U (2005) The surface and materials science of tin oxide. Prog Surf Sci 79:47–154
3. Batzill M, Diebold U (2007) Surface studies of gas sensing metal oxides. Phys Chem Chem Phys 9:2307
4. Batzill M (2006) Surface science studies of gas sensing materials: SnO_2. Sensors 6:1345
5. Wöll C (2007) The chemistry and physics of zinc oxide surfaces. Prog Surf Sci 82:55
6. Chevtchenko SA, Moore JC, Özgür U, Gu X, Baski AA, Morkoc H, Nemeth B, Nause JE (2006) Comparative study of the (0001) and (000–1) surfaces of ZnO. Appl Phys Lett 89:182111
7. Lahiri J, Senanayake S, Batzill M (2008) Soft x-ray photoemission of clean and sulfur-covered polar ZnO surfaces: a view of the stabilization of polar oxide surfaces. Phys Rev B 78:155414
8. Dulub O, Diebold U, Kresse G (2003) Novel stabilization mechanism on polar surfaces: ZnO(0001)-Zn. Phys Rev Lett 90:016102
9. Bagus PS, Illas F, Pacchioni G, Parmigiani F (1999) Mechanisms responsible for chemical shifts of core-level binding energies and their relationship to chemical bonding. J Electron Spectrosc Relat Phenom 100:215
10. Kresse G, Dulub O, Diebold U (2003) Competing stabilization mechanism of the polar ZnO(0001)-Zn surface. Phys Rev B 68:245409
11. Önsten A, Stoltz D, Palmgren P, Yu S, Göthelid M, Karlsson UO (2010) Water adsorption on ZnO(0001): transition from triangular surface structure to a disordered hydroxyl terminated phase. J Phys Chem C 114:11157
12. Valtiner M, Torrelles X, Pareek A, Borodin S, Gies H, Grundmeier G (2010) In Situ study of the polar ZnO(0001)-Zn surface in Alkaline electrolytes. J Phys Chem C 114:15440
13. Kunat M, Gil Girol S, Becker T, Burghaus U, Wöll C (2002) Stability of the polar surfaces of ZnO: A reinvestigation using He-atom scattering. Phys Rev B 66:081402
14. Meyer B, Marx D (2003) Density-functional study of the structure and stability of ZnO surfaces. Phys Rev B 67:035403
15. Piper LFJ, Preston ARH, Fedorov A, Cho SW, DeMasi A, Smith KE (2010) Direct evidence of metallicity at ZnO(000–1)-(1 × 1) surfaces from angle resolved photoemission spectroscopy. Phys Rev B 81:233305
16. Ozawa K, Mase K (2010) Metallization of ZnO(10–10) by adsorption of hydrogen, methanol, and water: angle-resolved photoelectron spectroscopy. Phys Rev B 81:205322
17. Li L, King DL (2006) H2S removal with ZnO during fuel processing for PEM fuel cell applications. Catal Today 116:537–541
18. Lahiri J, Batzill M (2008) Surface functionalizationSurface functionalization of ZnO photocatalysts with monolayer ZnS. J Phys Chem C 112:4304
19. Knop-Gericke A, Kleimenov E, Haevecker M, Blume R, Teschner D, Zafeiratos S, Schloegl R, Bukhtiyarov VI, Kaichev VV, Prosvirin IP, Nizovskii AI, Bluhm H, Barinov A, Dudin P,

Kiskinova M (2009) X-Ray photoelectron spectroscopy for investigation of heterogeneous catalytic processes. Adv Catal 52:213
20. Zhang C, Grass ME, McDaniel AH, DeCaluwe SC, El Gabaly F, Liu Z, McCarty KF, Farrow RL, Linne MA, Hussain Z, Jackson GS, Bluhm H, Eichhorn BW (2010) Measuring fundamental properties in operating solid oxide electrochemical cells by using in situ X-ray photoelectron spectroscopy. Nature Mat. 9:944
21. Diebold U (2003) The surface science of titanium dioxide. Surf Sci Rep 48:53
22. Liang Y, Gan SP, Chambers SA, Altman EI (2001) Surface structure of anatase TiO_2(001): reconstruction, atomic steps, and domains. Phys Rev B 63:235402
23. Chambers SA, Wang CM, Thevuthasan S, Droubay T, McCready DE, Lea AS, Shutthanandan V, Windisch CF (2002) Epitaxial growth and properties of MBE-grown ferromagnetic Co-doped TiO_2 anatase films on $SrTiO_3$(001) and $LaAlO_3$(001). Thin Solid Films 418:197
24. Dohnálek Z, Lyubinetsky I, Rousseau R (2010) Thermally-driven processes on rutile TiO_2(110)-1 × 1: a direct view at the atomic scale. Prog Surf Sci 85:161
25. Torrelles X, Cabailh G, Lindsay R, Bikondoa O, Roy J, Zegenhagen J, Teobaldi G, Hofer WA, Thornton G (2008) Geometric structure of TiO_2(011)(2 × 1). Phys Rev Lett 101:185501
26. Gong X-Q, Khorshidi N, Stierle A, Vonk V, Ellinger C, Dosch H, Cheng H, Selloni A, He Y, Dulub O, Diebold U (2009) The 2 × 1 reconstruction of the rutile TiO_2(011) surface: a combined density functional theory, X-ray diffraction, and scanning tunneling microscopy study. Surf Sci 603:138
27. He Y, Li W-K, Gong X-Q, Dulub O, Selloni A, Diebold U (2009) Nucleation and growth of 1D water clusters on Rutile TiO_2 (011)-2 × 1. Phys Chem C 113:10329–10332
28. Beck TJ, Klust A, Batzill M, Diebold U, Di Valentin C, Selloni A (2004) Surface structure of TiO_2(011)-(2 × 1). Phys Rev Lett 93:036104
29. Guo Q, Cocks I, Williams EM (1997) The orientation of acetate on a TiO_2(110) surface. J Chem Phys 106:2924
30. Thevuthasan S, Herman GS, Kim YJ, Chambers SA, Peden CHF, Wang Z, Ynzunza RX, Tober ED, Morais J, Fadley CS (1998) The structure of formate on TiO_2(110) by scanned-energy and scanned-angle photoelectron diffraction. Surf Sci 401:261
31. Gutierrez-Sosa A, Martinez-Escolano P, Raza H, Lindsay R, Wincott PL, Thornton G (2001) Orientation of carboxylates on TiO_2(110). Surf Sci 471:163
32. Bates SP, Kresse G, Gillan MJ (1998) The adsorption and dissociation of ROH molecules on TiO_2(110). Surf Sci 409:336
33. Onishi H, Iwasawa Y (1996) STM observation of surface reactions on a metal oxide. Surf Sci 357:773
34. Tao J, Luttrell T, Bylsma J, Batzill M (2011) Adsorption of acetic acid on rutile TiO_2(110) vs (011)-2 × 1 surfaces. J Phys Chem C 115:3434
35. Henrich VE, Dresselhaus G, Zeiger HJ (1976) Observation of two-dimensional phases associated with defect states on the surface of TiO_2. Phys RevLett 36:1335
36. Henderson MA, Epling WS, Peden CHF, Perkins CL (2003) Insights into photoexcited electron scavenging processes on TiO_2 obtained from studies of the reaction of O_2 with OH groups adsorbed at electronic defects on TiO_2(110). J Phys Chem B 107:534–545
37. Kurtz RL, Stockbauer R, Madey TE, Roman E, Desegovia JL (1989) Synchrotron radiation studies of H_2O adsorption on TiO_2(110). Surf Sci 218:178
38. Zhang Z, Jeng S-P, Henrich VE (1991) Cation-ligand hybridization for stoichiometric and reduced TiO_2 (110) surfaces determined by resonant photoemission. Phys Rev B 43:12004
39. Bao S, Liu G, Woodruff DP (1988) Angle-resolved polarised light photoemission study of the formation and structure of acetate on Cu(110). Surf Sci 203:89
40. Karis O, Hasselstrom J, Wassdahl N, Weinelt M, Nilsson A, Nyberg M, Pettersson LGM, Stohr J, Samant MG (2000) The bonding of simple carboxylic acids on Cu(110). J Chem Phys 112:8146

41. Tao J, Batzill M (2010) Role of surface structure on the charge trapping in TiO_2 photocatalysts. J Phys Chem Lett 1:3200
42. Redinger A, Hansen H, Linke U, Rosandi Y, Urbassek HM, Michely T (2006) Superior regularity in erosion patterns by planar subsurface channeling. Phys Rev Lett 96:106103
43. Redinger A, Rosandi Y, Urbassek HM, Michely T (2008) Step-edge sputtering through grazing incidence ions investigated by scanning tunneling microscopy and molecular dynamics simulations. Phys Rev B 77:195436
44. Luttrell T, Batzill M (2010) Nanoripple formation on TiO_2(110) by low-energy grazing incidence ion sputtering. Phys Rev B 82:035408
45. Gong XQ, Selloni A, Batzill M, Diebold U (2006) Steps on anatase TiO_2(101). Nat Mater 5:665
46. Luttrell T, Li WK, Gong XQ, Batzill M (2009) New directions for atomic steps: step alignment by grazing incident ion beams on TiO_2(110). Phys Rev Lett 102:166103
47. Li M, Hebenstreit W, Gross L, Diebold U, Henderson MA, Jennison DR, Schultz PA, Sears MP (1999) Oxygen-induced restructuring of the TiO_2(110) surface: a comprehensive study. Surf Sci 437:173
48. Bowker M, Bennett RA (2009) The role of Ti^{3+} interstitials in TiO_2(110) reduction and oxidation. J Phys Condens Matt 21:474224
49. Stone P, Bennett RA, Bowker M (1999) Reactive re-oxidation of reduced TiO_2(110) surfaces demonstrated by high temperature STM movies. New J Phys 1:8
50. McCarty KF (2003) Growth regimes of the oxygen-deficient TiO_2(110) surface exposed to oxygen. Surf Sci 543:185
51. Tao J, Luttrell T, Batzill M (2011) A two-dimensional phase of TiO_2 with a reduced bandgap. Nat Chem 3:296
52. Gurlo Nanosensors A (2010) Does crystal shape matter? Small 6:2077

http://www.springer.com/978-1-4614-5394-9

Metal Oxide Nanomaterials for Chemical Sensors
Carpenter, M.A.; Mathur, S.; Kolmakov, A. (Eds.)
2013, XX, 548 p., Hardcover
ISBN: 978-1-4614-5394-9